Fuel Processing Technology 119 (2014) 67–73

Contents lists available at ScienceDirect

Fuel Processing Technology

journal homepage: www.elsevier.com/locate/fuproc

Ce–Mn mixed oxides as supports of copper- and nickel-based catalysts for water–gas shift reaction

Eduardo Poggio Fraccari [a], Oriana D'Alessandro [b], Jorge Sambeth [b], Graciela Baronetti [a], Fernando Mariño [a,*]

[a] Laboratorio de Procesos Catalíticos, Pabellón de Industrias, Ciudad Universitaria, Universidad de Buenos Aires, Buenos Aires, Argentina
[b] CINDECA-CCT CONICET La Plata, Facultad de Ciencias Exactas, UNLP, La Plata, Argentina

ARTICLE INFO

Article history:
Received 12 January 2013
Received in revised form 11 July 2013
Accepted 23 October 2013
Available online xxxx

Keywords:
Water–gas shift reaction
Copper
Nickel
Cerium
Manganese
Fuel cells

ABSTRACT

Cerium-manganese mixed oxides with different composition were prepared by co-precipitation, characterized and evaluated for the water–gas shift (WGS) reaction. Base metal (5 wt.% Cu and 5 wt.% Ni) catalysts supported on Ce–Mn mixed oxides were also tested for the WGS reaction. The activity of the bare supports is higher in the mixed samples than in pure ceria or manganese oxide. This result can be explained by a combination of greater reducibility and surface area in the mixed samples. Addition of base metals produces superior WGS catalysts. Particularly, nickel catalysts tested are able to reduce typical CO concentrations entering the WGS process to the CO levels tolerated by phosphoric acid fuel cells in a single unit operated at 400 °C.

© 2013 Elsevier B.V. All rights reserved.

1. Introduction

During the 20th century, a strong development of industry and transportation as well as the improvement of the living standards has forced an important increase in the global energy consumption. In particular, CO_2 emissions in a per capita basis augmented more than 10 times during 20th century, as a result of a striking increase in the worldwide consumption of fossil fuels [1]. The use of devices more efficient for energy conversion, such as fuel cells, is one of the advisable alternatives for reducing the energy consumption and the greenhouse gas emissions. High temperature fuel cells, such as molten carbonate fuel cells (MCFC) or solid oxide fuel cells (SOFC), can be fueled with a hydrogen stream also containing carbon oxides or water. Nevertheless, CO must be partially removed from the feed in the case of fuel cells that operates at lower temperatures, like phosphoric acid fuel cells (PAFC) or proton-exchange membrane fuel cells (PEMFC). Hence, in the case of low temperature fuel cells, hydrogen produced by reforming or partial oxidation of a carbon containing raw material (alcohols or hydrocarbons) must be purified in order to reduce CO levels to cell requirements. In the case of PAFC, CO removal in a water–gas shift (WGS) reactor is sufficient to obtain a CO concentration of approximately 1-2%, which can be tolerated by the fuel cell. PEMFC are extremely sensitive to the presence of CO and the product stream from WGS unit must be further purified to less than 20 ppm for a stable operation [2,3].

The water gas shift reaction (Eq. (1)) was first reported in 1888, but it came into popular usage later, as a source of hydrogen for the Haber process for the manufacture of ammonia [4].

$$CO(g) + H_2O(g) = CO_2(g) + H_2(g) \quad \Delta H^0_{298} = -41.1\ \text{kJ/mol} \qquad (1)$$

Water–gas shift reaction has been extensively used in large chemical and petrochemical plants for many years; in such processes, WGS reactor is placed after the reformer unit to adjust CO levels in the syngas to the H_2/CO ratio suitable for a particular application, or simply to increase the H_2 yield and decrease the CO concentration, which is a poison for some catalysts used downstream like in ammonia synthesis or oil dehydrogenation. Recently, non-traditional applications of hydrogen such as electric power generation in fuel cells have given rise to new research efforts pointed to find active and stable catalysts for the WGS. Among these works, several authors, taking into account the redox properties and the oxygen storage capacity of ceria, propose ceria-supported noble metal catalysts [5–9] or less expensive ceria-supported base metal catalysts [10–14]. Copper-manganese spinel oxides have shown excellent WGS activity, comparable to that of conventional LTWGS catalysts despite its low surface area [15]. Manganese oxide is itself a proven catalyst, in oxidation–reduction reactions, such as, for example, the oxidation of methane and CO [16]. Manganese, which exhibits a multiplicity of oxidation states, is also a good candidate to make part of a ceria-based partially reducible support [17] for redox reactions such as WGS [18,19] or CO preferential oxidation [20].

* Corresponding author at: Laboratorio de Procesos Catalíticos, Departamento de Ingeniería Química, Facultad de Ingeniería, Universidad de Buenos Aires, Pabellón de Industrias, Ciudad Universitaria, (1428) Buenos Aires, Argentina. Tel.: +54 11 45763240; fax: +54 11 45763241.

0378-3820/$ – see front matter © 2013 Elsevier B.V. All rights reserved.
http://dx.doi.org/10.1016/j.fuproc.2013.10.012

In the present article, cerium–manganese mixed oxides were co-precipitated, characterized and evaluated in the WGS reaction. These solids were also used as supports to prepare impregnated copper or nickel catalysts. In this way, the present work aims to obtain cost-effective base metal catalysts supported on Ce–Mn mixed oxides, suitable for WGS reaction in fuel cell applications.

2. Experimental

2.1. Catalyst preparation

The precursors of the manganese-cerium mixed oxides were prepared by co-precipitation technique from aqueous solutions of metallic salts $Ce(NO_3)_3$ 0.1 M (Fluka) and $Mn(NO_3)_2.4H_2O$ 2M (Sigma-Aldrich) in basic medium at room temperature, according to Inamura et al. [21], using NaOH 3M as precipitant agent. The solids were prepared with the several Mn/Ce atomic ratios. The obtained samples were washed with bi-distilled water until the presence of Na cations is not further detected. Then, they were dried at 100 °C and calcined at 450 °C in air atmosphere for 5 h. The nomenclature used for describing cerium–manganese mixed oxides is CeMnX, where X is the atomic fraction of manganese. Then, samples CeMn0 (CeO_2), CeMn30, CeMn50, CeMn70 and CeMn100 (MnOx) are studied throughout the work.

A portion of samples CeMn30 and CeMn50 were impregnated with Cu^{2+} or Ni^{2+} salts ($Cu(NO_3)_2.3H_2O$ from Sigma-Aldrich or $Ni(NO_3)_2.6H_2O$ from Merck, respectively) to give 5 Cu wt.% or 5 Ni wt.% catalysts supported on Ce–Mn mixed oxides. The supports were in contact with a solution of Cu or Ni nitrates in constant agitation for 5 hours at room temperature. Then, the obtained slurry was filtered, the solid dried overnight at 70 °C and subsequently calcined in air following the same procedure as the Ce–Mn oxides.

2.2. Characterization

The specific BET surface of the samples was measured in a Sortometer Micromeritics ASAP 2020. Solids were also analyzed by X-ray Diffraction (XRD) in a Philips PW 1390 equipment with radiation corresponding to CuKα. Temperature-Programmed Reduction experiments were performed in a Quantachrome Quantasorb Jr. apparatus using an H_2/N_2 stream (5% H_2, total flow: 20 cm^3/min) and 20 mg of the sample, while operation temperature was raised following a ramp rate of 20 °C/min.

2.2.1. WGS activity tests

Activity tests were conducted in an isothermal fixed bed glass reactor heated with an electrical oven. The catalytic performance was evaluated at several temperatures in the range 250–450 °C. In a typical test, 120 mg of catalyst and a total inlet flow of 150 cm^3/min are employed; in the case of bare supports, tests were performed with 240 mg of catalyst and a total gas flow of 85 cm^3/min. Before each analysis the solids were reduced during 30 minutes with a H_2 stream (50% of H_2 in N_2) at the higher temperature of reaction (450 °C). At the reactor outlet, analysis of non-converted CO and gaseous products was performed by a Hewlett Packard HP 6890 gas chromatograph equipped with a TCD detector. CO conversion is conventionally defined by Eq. (2). Considering that methanation could occur, selectivity towards CO_2 is defined through Eq. (3).

$$x = \frac{F_{CO}^{in} - F_{CO}^{out}}{F_{CO}^{in}} \quad (2)$$

$$S = \frac{F_{CO2}^{out}}{F_{CO}^{in} - F_{CO}^{out}} \quad (3)$$

where F_i^{in} and F_i^{out} are the inlet and outlet molar flow of gas i, respectively.

Reported values of CO conversion and selectivity correspond to steady state values.

3. Results and discussion

3.1. Cerium–manganese mixed oxides

BET surface areas of CeMnX samples are reported in Table 1. It can be noted that surface area values pass through a maximum with respect to the composition of the Ce–Mn mixed oxides. Manganese oxide presents the lowest BET area (17 m^2/g) and the equimolar CeMn50 sample has the highest value (69 m^2/g). A similar behavior was found by Chen et al. [22]. Comparison of these results with some of our previous works on samples calcined at a lower temperature (350 °C) reveals a strong influence of the thermal treatment in this temperature range. In effect, BET area drops from 137 m^2/g in ceria calcined at 350 °C to 50 m^2/g in ceria calcined at 450 °C and from 22 m^2/g in MnOx calcined at 350 °C to 17 m^2/g at 450 °C [23].

Fig. 1 presents XRD patterns of the solids analyzed in this work. Pure ceria (CeMn0) pattern shows the peaks corresponding to the face-centered cubic fluorite-type structure typical of CeO_2.

Comparison of XRD patterns of CeO_2 and Ce–Mn mixed oxides reveals a partial substitution of Mn into ceria lattice. In effect, reflections of ceria shift to higher 2θ angles in the mixed oxides due to the lower atomic radius of manganese with respect to cerium. On the other hand, different manganese phases are found in the patterns of mixed samples compared to pure manganese oxide. Thus, as it is exposed in Fig. 1, MnO_2 phase is only present in cerium containing samples, while the Mn_3O_4 phase (i.e. $MnO.Mn_2O_3$) is only observed in sample CeMn100. As it can be concluded, the presence of cerium stabilizes phases involving higher oxidation states of manganese after calcination of mixed samples at 450 °C.

Fig. 2 shows the H_2-TPR profiles of the CeMn supports studied in this work. It can be seen that the reduction behavior of ceria (CeMn0 sample) is completely different than those of the Ce–Mn mixed samples. In fact, reduction profile of ceria is characterized by a typical bimodal curve that presents the first reduction event between 400 °C and 600 °C and the second event between 700 °C and 900 °C. The first peak is usually assigned to H_2 consumption during the surface reduction process whereas the second one is related to bulk ceria reduction [24,25]. The extension of the reduction for ceria sample is markedly lower than those of manganese oxide or Ce–Mn mixed samples, as it can be seen from the H_2 consumption in the whole temperature range (100–900 °C) reported in Table 1. Ce–Mn mixed oxides exhibit a reduction profile similar of that of pure manganese oxide, even for the lowest Mn content analyzed. In these cases, two reduction peaks are present between 200 °C and 500 °C, which are named α (low temperature peak) and β (high temperature peak). Similar reduction profiles were reported in the literature. Although Hamoudi et al. [26] attributed the α peak to the reduction of manganese oxide and β peak to the reduction of ceria, the reduction events observed in the 200–500 °C temperature range were assigned to manganese oxide species and not to cerium reduction by most of the authors; moreover, α and β peaks were ascribed to the step reduction of species with different Mn oxidation states [27–30]. H_2-TPR profiles of Mn_2O_3 reported by Morales et al. [30] exhibit two well-defined peaks, with maxima at 374 °C and 477 °C, that probably correspond to a step reduction $Mn_2O_3 \rightarrow Mn_3O_4 \rightarrow MnO$. Carnö et al. [27] observed a TPR profile with three reduction events in their alumina-supported manganese oxides calcined at 500 °C. In this case, the first peak of hydrogen consumption was attributed to the $MnO_2 \rightarrow Mn_2O_3$ reduction step. Both works [27,30] agree that samples remain as MnO after TPR experiments since further reduction of MnO to metallic Mn only occurs at temperatures higher than 1200 °C. Chen et al. [22] also found TPR profiles featured by two main reduction events in pure manganese oxide or in

Table 1
BET area and H_2-TPR results of Ce–Mn mixed oxides.

Sample	BET area (m^2/g)	Total H_2-TPR consumption[a] (μmol)	H_2-TPR consumption (T < 450 °C) (μmol)	α Peak position (°C)	β Peak position (°C)	(β/α) area ratio
CeMn0	50	6.6	–	–	–	–
CeMn30	54	71.4	70.6	315	410	0.55
CeMn50	69	86.7	85.5	315	425	0.53
CeMn70	51	124.2	114.2	320	435	0.58
CeMn100	17	190.1	149.8	338	465	1.11

[a] Temperature range 100–900 °C.

manganese rich Mn-Ce mixed oxides; nevertheless, they also reported a slight shoulder at the reduction onset, probably corresponding to the first step reported by Carnö et al. [27], which could be misinterpreted in many TPR profiles [31]. Craciun et al. [29] working with MnOx/YSZ catalysts calcined at 800 °C reported a main peak of hydrogen consumption at 447 °C corresponding to the $Mn_3O_4 \rightarrow MnO$ final reduction, while the presence of small quantities of MnO_2 and Mn_2O_3 cannot be discarded. The position of α peaks in the H_2-TPR profiles of Fig. 2 is practically independent of the manganese content of the samples. As reported in Table 1, maxima of these peaks are positioned in the temperature range 315–338 °C. A slight decrease in the temperature of the maximum H_2 consumption as the Ce content increases is observed, in agreement with the observations of Chen et al. [22]. It is shown in Table 1 that the position of β peaks also shift to lower temperatures as cerium content of the samples increases, being these changes more pronounced with respect to α peaks. From the above results, it can be concluded that the reducibility of the mixed oxides, mainly for the $Mn_3O_4 \rightarrow MnO$ reduction step, is enhanced by cerium addition that favours oxygen mobility [22]. The slight variation in the onset of α peaks might also be explained by the different surface area of the samples [32].

Table 1 also presents the ratio of β to α peak areas. As it can be seen, this ratio is faintly higher than 0.5 and approximately independent of sample composition for Ce–Mn mixed oxides, but (β/α) ratio doubles in the case of pure manganese oxide. Considering that the reduction steps proposed for the different manganese oxide species totally occur, theoretical (β/α) ratios can be calculated. If we assume that all the manganese is present as MnO_2 in the samples before TPR experiments, and that the bimodal profile is related to the consecutive steps $MnO_2 \rightarrow Mn_3O_4$ (α peak) and $Mn_3O_4 \rightarrow MnO$ (β peak), then (β/α) ratio should have the value 0.5. This is approximately the case of CeMn30, CeMn50 and CeMn70 samples where it can be assumed that most of the manganese added is in the Mn^{4+} oxidation state before TPR is performed. On the contrary, if we assume that the first reduction step is $Mn_2O_3 \rightarrow Mn_3O_4$ and the second one is $Mn_3O_4 \rightarrow MnO$, then stoichiometry determines that (β/α) ratio should be equal to 2. This last result indicates that a mixture of Mn^{2+}, Mn^{3+} and Mn^{4+}oxides might be found in the CeMn100 sample before TPR experiments. These conclusions are in good agreement with XRD observations previously presented.

The catalytic behavior of CeMnX samples for water–gas shift reaction was tested. CO conversion obtained at the outlet of the experimental plug flow reactor is represented as a function of the operating temperature (Fig. 3). As it can be observed, mixed samples are more active than CeO_2 or MnOx samples. In particular, equimolar CeMn50 sample exhibits the best catalytic behavior in the whole temperature range analyzed.

Since samples are reduced in-situ at 450 °C before the catalytic runs, the amount of manganese reduced at this temperature can be estimated from the integration of TPR profiles in Fig. 2 up to 450 °C (see Table 1). As it can be seen, H_2-TPR consumption in the range 100–450 °C

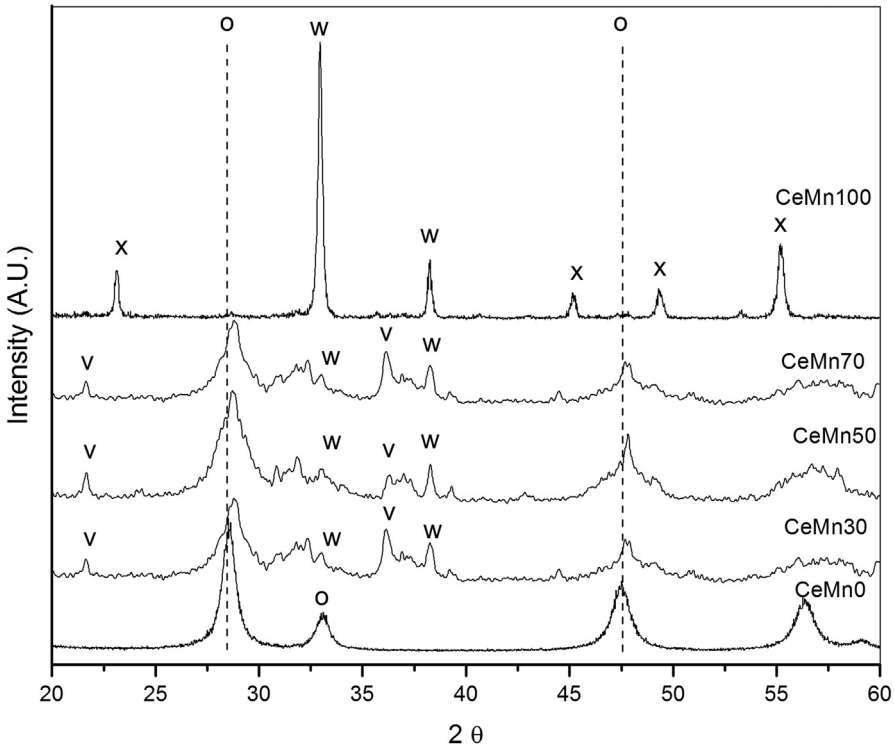

Fig. 1. XRD patterns of Ce–Mn mixed oxides. "x": Mn_3O_4 (ICDD file #18-0803); "w": Mn_5O_8 (ICDD file #39-1218); "v": MnO_2 (ICDD file #39-0375); "o": CeO_2 (ICDD file #34-0394).

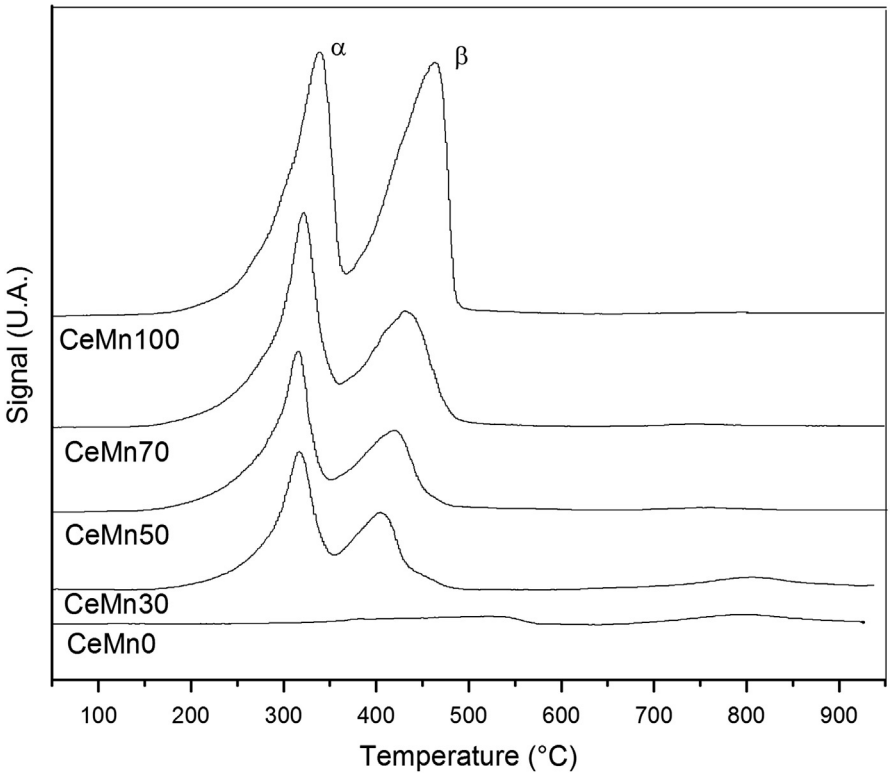

Fig. 2. H_2-TPR profiles of Ce–Mn mixed oxides.

increases as Mn content increases. However, Table 1 also exposes that surface area has a maximum as a function of Mn content of the sample and that BET area dramatically drops for the pure manganese oxide sample (CeMn100). Hence, the enhanced catalytic performance of mixed oxides could be attributed to the combination of both effects.

3.2. Copper and nickel catalysts supported on cerium–manganese mixed oxides

It has been reported that the activity of ceria-based materials for the WGS reaction is significantly improved by the addition of base metals, such as copper or nickel [33]. In addition, some of our previous results have also shown that, among several base metals analyzed, copper and nickel catalysts supported on ceria-based oxides are extremely active for CO oxidation by O_2 under COPROX conditions [34]. Taking this background into account, copper and nickel catalysts (5 wt.%) supported on some of the cerium-manganese mixed oxides described in the previous section were considered for the WGS reaction.

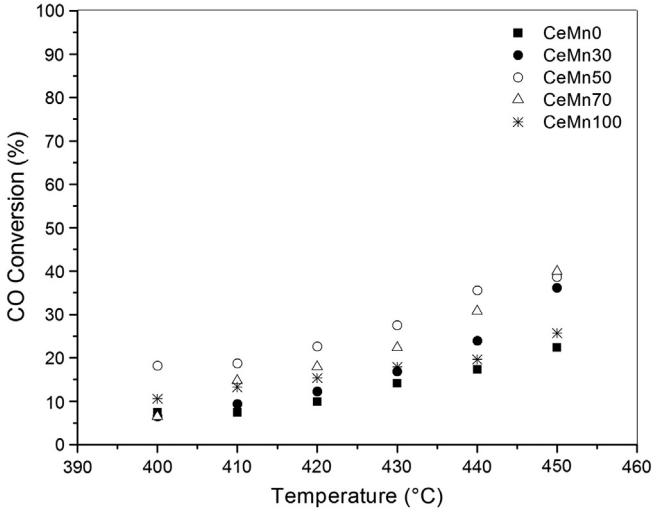

Fig. 3. Catalytic activity of Ce–Mn mixed oxides for the WGS reaction. Catalytic mass = 240 mg. Gas flow = 85 ml min^{-1}. Feed composition: 8% CO, 24% H_2O, N_2 as balance.

XRD patterns of copper catalysts prepared in this work are presented in Fig. 4. XRD patterns suggest the presence of a small amount of copper segregated as tenorite (ICDD file #45-0937) in both samples: Cu/CeMn30 and Cu/CeMn50. Fig. 5 shows the XRD patterns of Ni/CeMn30 and Ni/CeMn50 catalysts. In this case, typical signals of a segregated bunsenite phase (ICDD file #47-1049) are not distinguished in the XRD patterns. In both cases, copper and nickel catalysts, comparison of XRD patterns with those of the corresponding supports (Fig. 1) indicates that there are not structural changes in the Ce–Mn mixed oxides after metal impregnation and subsequent calcination.

Water–gas shift activity of copper and nickel catalysts is displayed in Figs. 6 and 7 respectively. Comparison of Figs. 6 and 7 with Fig. 3 reveals that the activity of copper or nickel catalysts is markedly higher than that of the corresponding supports. For example taking copper samples, it can be noted that CO conversions with catalysts or supports are similar to those obtained with the bare supports although the contact time used in Fig. 3 is 3.5 times larger than in Fig. 6.

Comparing Fig. 6 with Fig. 7 it is evident that the activity of copper samples is lower than that of nickel catalysts. In effect, maximal CO conversion attained with the most active copper sample (Cu/CeMn30) is slightly higher than 40%. On the other hand, both nickel catalysts evaluated are able to reach CO conversions higher than 80%. Curves of CO conversion vs. T curves for Ni catalysts are steeper and with a higher light-off temperature (Fig. 7) with respect to the curves of copper catalysts (Fig. 6). These results are in good agreement with those presented by other authors [33,35,36] predicting a higher activation energy in the case of nickel catalysts.

It must be mentioned that methane is detected at the reactor outlet when the reaction is carried out with nickel catalysts. As it is known,

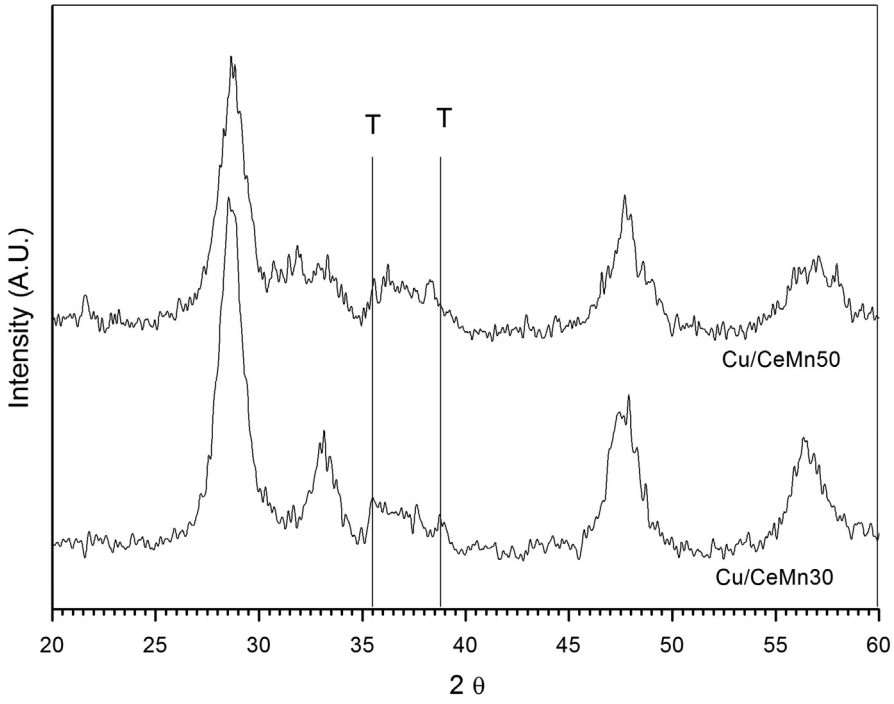

Fig. 4. XRD patterns of Cu/CeMn30 and Cu/CeMn50 catalysts. "T": Tenorite (CuO) signals at 2θ = 35.5º and 38.8º.

nickel is an effective catalyst for methanation reactions [37,38]. In particular, nickel catalysts supported on ceria-based oxides have demonstrated high activity for CO methanation (Eq. (4)) in reformate gas [39,40].

$$CO(g) + 3H_2(g) = CH_4(g) + H_2O(g) \quad \Delta H^0_{298} = -206\ \text{kJ/mol} \qquad (4)$$

CO methanation helps to reduce CO concentration in the H_2 stream but, at the same time, this reaction consumes 3 moles of H_2 for each mole of CO. As a consequence, selectivity (as defined by Eq. (3)) should be higher than 0.75 to avoid hydrogen loss in the WGS reactor. Fig. 8 presents selectivity values in the temperature range 300-400 °C for both nickel catalysts tested in this work. Selectivity values are presented for operating temperatures lower than 400 °C because, as shown in

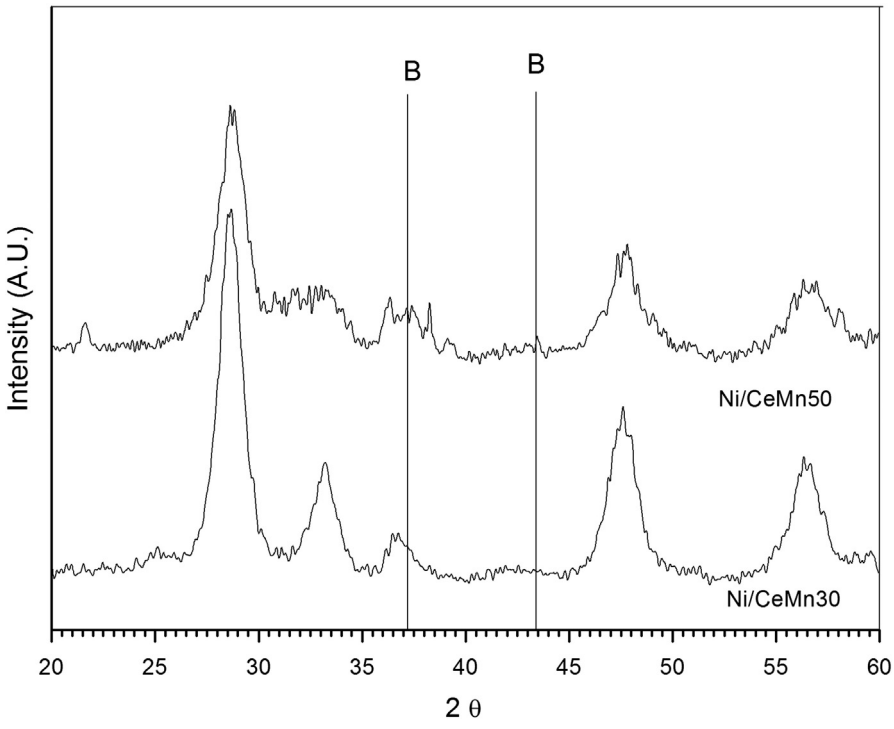

Fig. 5. XRD patterns of Ni/CeMn30 and Ni/CeMn50 catalysts. "B": Bunsenite (NiO) signals at 2θ = 37.2° and 43.3°.

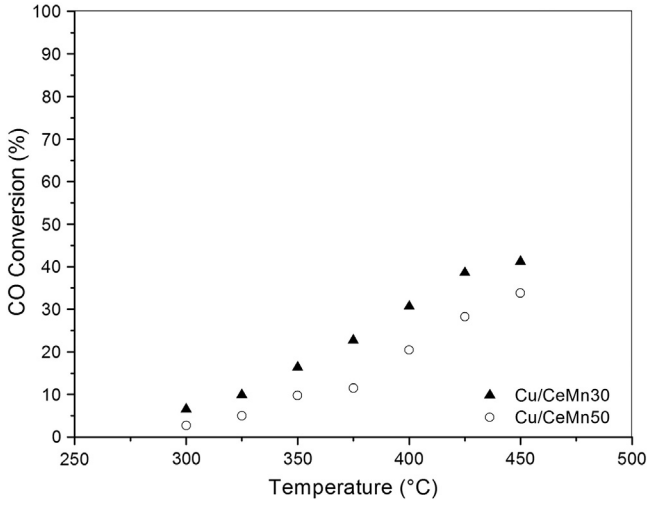

Fig. 6. Activity of Cu/CeMn30 and Cu/CeMn50 catalysts for the WGS reaction Catalytic mass = 120 mg. Gas flow = 150 ml min^{-1}. Feed composition: 8% CO, 24% H_2O, 45% H_2, N_2 as balance.

Fig. 7, CO conversion diminishes above 400 °C due to the limitations imposed by thermodynamic equilibrium. It can be observed in Fig. 8 that selectivity is higher for the catalyst supported on the oxide with higher cerium content (Ni/CeMn30). As expected, selectivity decreases with reaction temperature for both catalysts. Finally, it should be noted that all the values presented in Fig. 8 are close or higher than 0.75, indicating that hydrogen consumption is not important in any case.

4. Conclusions

The activity of cerium–manganese mixed oxides for the WGS reaction in the temperature range 400–450 °C is markedly higher than that of pure CeO_2 or MnOx. XRD and TPR results revealed that Ce–Mn mixed oxides contain a greater proportion of Mn^{4+} species than pure MnO_x. The superior catalytic behavior of Mn–Ce samples can be explained from a combination of two effects: a greater reducibility of manganese species during the in-situ activation at 450 °C and a higher surface area of mixed samples with respect to pure manganese oxide. Impregnation of Ce–Mn oxides with 5 wt.% copper or nickel results in

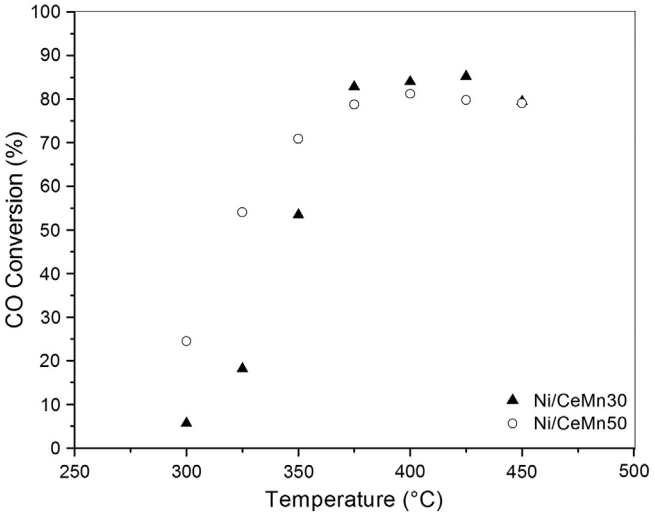

Fig. 7. Activity of Ni/CeMn30 and Ni/CeMn50 catalysts for the WGS reaction Catalytic mass = 120 mg. Gas flow = 150 ml min^{-1}. Feed composition: 8% CO, 24% H_2O, 45% H_2, N_2 as balance.

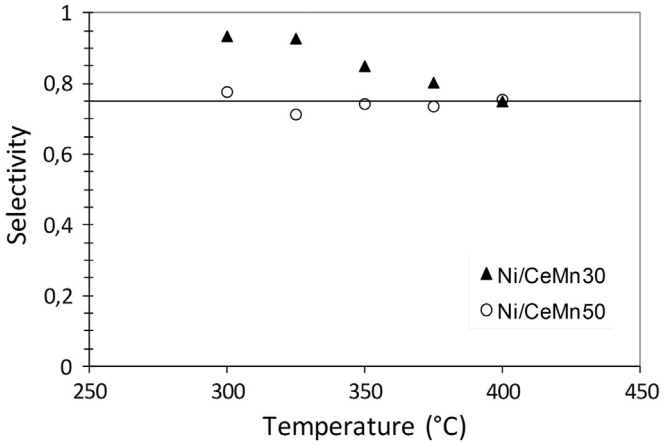

Fig. 8. Selectivity of Ni/CeMn30 and Ni/CeMn50 catalysts towards CO_2 production.

superior WGS catalysts compared to the corresponding bare supports. In particular, Ni catalysts operating at ca. 400 °C has shown to be capable of purifying a hydrogen stream from 8%CO to less than 2%CO, which can be tolerated by a PAFC, even generating additional H_2.

References

[1] Ch. Song, Fuel processing for low-temperature and high-temperature fuel cells. Challenges and opportunities for sustainable development in the 21st century, Catalysis Today 77 (2002) 17–49.
[2] Fuel Cell Handbook, 7th ed. US Department of Energy, Office of Fossil Energy, National Energy Technology Laboratory, Morgantown, WV, 2004.
[3] S. Ahmed, M. Krumpelt, Hydrogen from hydrocarbon fuels for fuel cells, International Journal of Hydrogen Energy 26 (2001) 291–301.
[4] Ch. Ratnasamy, J. Wagner, Water gas shift catalysis, Catalysis Reviews: Science and Engineering 51 (2009) 325–440.
[5] T. Bunluesin, R.J. Gorte, G.W. Graham, Studies of the water-gas-shift reaction on ceria-supported Pt, Pd, and Rh: implications for oxygen-storage properties, Applied Catalysis B: Environmental 15 (1998) 107–114.
[6] R.J. Gorte, S. Zhao, Studies of the water–gas-shift reaction with ceria-supported precious metals, Catalysis Today 104 (2005) 18–24.
[7] A. El-Moemen, A. Karpenko, Y. Denkwitz, R. Behm, Activity stability and deactivation of Au/CeO_2 catalysts in the water gas shift reaction at increased reaction temperature (300 °C), Journal of Power Sources 190 (2009) 64–75.
[8] K.R. Hwang, J.S. Park, S.K. Ihm, Si-modified Pt/CeO_2 catalyst for a single-stage water–gas shift reaction, International Journal of Hydrogen Energy 36 (2011) 9685–9693.
[9] P. Panagiotopoulou, D. Kondarides, A comparative study of the water-gas shift activity of Pt catalysts supported on single (MO_x) and composite (MO_x/Al_2O_3, MO_x/TiO_2) metal oxide carriers, Catalysis Today 127 (2007) 319–329.
[10] P.V.D.S. Gunawardana, H.C. Lee, D.H. Kim, Performance of copper–ceria catalysts for water gas shift reaction in medium temperature range, International Journal of Hydrogen Energy 34 (2009) 1336–1341.
[11] N. Schumacher, A. Boisen, S. Dahl, A.A. Gokhale, S. Kandoi, L.C. Grabow, J.A. Dumesic, M. Mavrikakis, I. Chorkendorff, Trends in low-temperature water–gas shift reactivity on transition metals, Journal of Catalysis 229 (2005) 265–275.
[12] A.S. Quiney, Y. Schuurman, Kinetic modelling of CO conversion over a Cu/ceria catalyst, Chemical Engineering Science 62 (2007) 5026–5032.
[13] S. Natesakhawat, X. Wang, L. Zhang, U.S. Ozkan, Development of chromium-free iron-based catalysts for high-temperature water-gas shift reaction, Journal of Molecular Catalysis A: Chemical 260 (2006) 82–94.
[14] T. Tabakova, V. Idakiev, J. Papavasiliou, G. Avgouropoulos, T. Ioannides, Effect of additives on the WGS activity of combustion synthesized CuO/CeO_2 catalysts, Catalysis Communications 8 (2007) 101–106.
[15] Y. Tanaka, T. Utaka, R. Kikuchi, T. Takeguchi, K. Sasaki, K. Eguchi, Water gas shift reaction for the reformed fuels over Cu/MnO catalysts prepared via spinel-type oxide, Journal of Catalysis 215 (2003) 271–278.
[16] E. Hapeshi, C.R. Theocharis, Preparation and characterization of nanoporous solids with composition $Ce_xMn_{1-x}O_{2-y}$ with x values 0 to 1, Studies in Surface Science and Catalysis 160 (2007) 645–650.
[17] M. Ribeiro, G. Jacobs, U.M. Graham, K.G. Azzam, L. Linganiso, B.H. Davis, Low temperature water–gas shift: differences in oxidation states observed with partially reduced Pt/MnO_X and Pt/CeO_X catalysts yield differences in OH group reactivity, Catalysis Communications 11 (2010) 193–199.
[18] L. Jiang, B. Ye, K. Wei, Effects of CeO_2 on structure and properties of Ni–Mn–K/bauxite catalysts for water–gas shift reaction, Journal of Rare Earths 26 (2008) 352–356.
[19] X. Du, Z. Yuan, L. Cao, Ch. Zhang, Sh. Wang, Water gas shift reaction over Cu–Mn mixed oxides catalysts: effects of the third metal, Fuel Processing Technology 89 (2008) 131–138.

[20] Q. Guo, Y. Liu, MnO_x modified Co_3O_4–CeO_2 catalysts for the preferential oxidation of CO in H_2-rich gases, Applied Catalysis B: Environmental 82 (2008) 19–26.
[21] S. Inamura, A. Dol, S. Ishida, Industrial and Engineering Chemistry Product Research and Development 24 (1985) 75–80.
[22] H. Chen, A. Sayari, A. Adnot, F. Larachi, Composition–activity effects of Mn–Ce–O composites on phenol catalytic wet oxidation, Applied Catalysis B: Environmental 32 (2001) 195–204.
[23] O. D'Alessandro, Study of Phenol Adsorption–Oxidation Mechanism on the Catalytic System Mn–Ce–O, (PhD Thesis) University of La Plata, Argentina, 2012.
[24] F. Giordano, A. Trovarelli, C. de Leitenburg, M. Giona, A model for the temperature-programmed reduction of low and high surface area ceria, Journal of Catalysis 193 (2000) 273–282.
[25] E. Poggio, M. Jobbagy, M. Moreno, M. Laborde, F. Mariño, G.T. Baronetti, Influence of the calcination temperature on the structure and reducibility of nanoceria obtained from crystalline $Ce(OH)CO_3$ precursor, International Journal of Hydrogen Energy 36 (2011) 15899–15905.
[26] S. Hamoudi, A. Sayari, K. Belkacemi, L. Bonneviot, F. Larachi, Catalytic wet oxidation of phenol over $Pt_xAg_{1-x}MnO_2/CeO_2$ catalysts, Catalysis Today 62 (2000) 379–388.
[27] J. Carnö, M. Ferrandon, E. Björnbom, S. Järas, Mixed manganese oxide/platinum catalysts for total oxidation of model gas from wood boilers, Applied Catalysis A: General 155 (1997) 265–281.
[28] S.T. Hussain, A. Sayari, F. Larachi, Enhancing the stability of Mn–Ce–O WETOX catalysts using potassium, Applied Catalysis B: Environmental 34 (2001) 1–9.
[29] R. Craciun, B. Nentwick, K. Hadjiivanov, H. Knözinger, Structure and redox properties of MnO_x/Yttrium-stabilized zirconia (YSZ) catalyst and its used in CO and CH_4 oxidation, Applied Catalysis A: General 243 (2003) 67–79.
[30] M.R. Morales, B.P. Barbero, L.E. Cadús, Total oxidation of ethanol and propane over Mn–Cu mixed oxide catalysts, Applied Catalysis B: Environmental 67 (2006) 229–236.
[31] M. Ferrandon, J. Carnö, S. Järas, E. Björnbom, Total oxidation catalysts based on manganese or copper oxides and platinum or palladium I: characterisation, Applied Catalysis A: General 180 (1999) 141–151.
[32] E.R. Stobbe, B.A. de Boer, J.W. Geus, The reduction and oxidation behaviour of manganese oxides, Catalysis Today 47 (1999) 161–167.
[33] Y. Li, Q. Fu, M. Flytzani-Stephanopoulos, Low-temperature water–gas shift reaction over Cu- and Ni-loaded cerium oxide catalysts, Applied Catalysis B: Environmental 27 (2000) 179–191.
[34] F. Mariño, C. Descorme, D. Duprez, Supported base metal catalysts for the preferential oxidation of carbon monoxide in the presence of excess hydrogen (PROX), Applied Catalysis B: Environmental 58 (2005) 175–183.
[35] J.H. Lin, P. Biswas, V.V. Guliant, S. Misture, Hydrogen production by water–gas shift reaction over bimetallic Cu–Ni catalysts supported on La-doped mesoporous ceria, Applied Catalysis A: General 387 (2010) 87–94.
[36] G. Jacobs, E. Chenu, P. Patterson, L. Williams, D. Sparks, G. Thomas, B. Davis, Water–gas shift: comparative screening of metal promoters for metal/ceria systems and role of the metal, Applied Catalysis A: General 258 (2004) 203–214.
[37] S. Takenaka, T. Shimizu, K. Otsuka, Complete removal of carbon monoxide in hydrogen-rich gas stream through methanation over supported metal catalysts, International Journal of Hydrogen Energy 29 (2004) 1065–1073.
[38] M. Krämer, M. Duisberg, K. Stöwe, W.F. Maier, Highly selective CO methanation catalysts for the purification of hydrogen-rich gas mixtures, Journal of Catalysis 251 (2007) 410–422.
[39] L. Wang, Sh. Zhang, Y. Liu, Reverse water gas shift reaction over co-precipitated Ni–CeO_2 catalysts, Journal of Rare Earths 26 (2008) 66–70.
[40] M.M. Zyryanova, P.V. Snytnikov, Yu.I. Amosov, V.A. Kuzmin, V.A. Kirillov, V.A. Sobyanin, Design, scale-out, and operation of a preferential CO methanation reactor with a nickel–ceria catalyst, Chemical Engineering Journal 176–177 (2011) 106–113.